OPEN

Citation: Cell Death and Disease (2013) 4, e626; doi:10.1038/cddis.2013.150

www.nature.com/cddis

# Protein tyrosine phosphatase 1B modulates GSK3β/Nrf2 and IGFIR signaling pathways in acetaminophen-induced hepatotoxicity

MA Mobasher[1,2], Á González-Rodriguez[1,2], B Santamaría[1,2], S Ramos[3], MÁ Martín[2,3], L Goya[3], P Rada[1,4], L Letzig[5], LP James[5], A Cuadrado[1,4], J Martín-Pérez[1], KJ Simpson[6], J Muntané[7,8] and AM Valverde*[,1,2]

**Acute hepatic failure secondary to acetaminophen (APAP) poisoning is associated with high mortality. Protein tyrosine phosphatase 1B (PTP1B) is a negative regulator of tyrosine kinase growth factor signaling. In the liver, this pathway confers protection against injury. However, the involvement of PTP1B in the intracellular networks activated by APAP is unknown. We have assessed PTP1B expression in APAP-induced liver failure in humans and its role in the molecular mechanisms that regulate the balance between cell death and survival in human and mouse hepatocytes, as well as in a mouse model of APAP-induced hepatotoxicity. PTP1B expression was increased in human liver tissue removed during liver transplant from patients for APAP overdose. PTP1B was upregulated by APAP in primary human and mouse hepatocytes together with the activation of c-jun (NH2) terminal kinase (JNK) and p38 mitogen-activated protein kinase (p38 MAPK), resulting in cell death. Conversely, Akt phosphorylation and the antiapoptotic Bcl2 family members BclxL and Mcl1 were decreased. PTP1B deficiency in mouse protects hepatocytes against APAP-induced cell death, preventing glutathione depletion, reactive oxygen species (ROS) generation and activation of JNK and p38 MAPK. APAP-treated PTP1B$^{-/-}$ hepatocytes showed enhanced antioxidant defense through the glycogen synthase kinase 3 (GSK3)β/Src kinase family (SKF) axis, delaying tyrosine phosphorylation of the transcription factor nuclear factor-erythroid 2-related factor (Nrf2) and its nuclear exclusion, ubiquitination and degradation. Insulin-like growth factor-I receptor-mediated signaling decreased in APAP-treated wild-type hepatocytes, but was maintained in PTP1B$^{-/-}$ cells or in wild-type hepatocytes with reduced PTP1B levels by RNA interference. Likewise, both signaling cascades were modulated in mice, resulting in less severe APAP hepatotoxicity in PTP1B$^{-/-}$ mice. Our results demonstrated that PTP1B is a central player of the mechanisms triggered by APAP in hepatotoxicity, suggesting a novel therapeutic target against APAP-induced liver failure.**

*Cell Death and Disease* (2013) **4,** e626; doi:10.1038/cddis.2013.150; published online 9 May 2013
**Subject Category:** Experimental Medicine

Acetaminophen (APAP) or paracetamol is a widely used analgesic and antipyretic, which is drug safe at therapeutic doses,[1] but accidental or intentional overdose induces severe hepatotoxicity in experimental animals and humans. APAP overdose is the most frequent cause of drug-induced liver failure in the United States[2,3] and most of Europe.[4,5] In these countries, APAP is a leading cause of urgent liver transplantation, which accounts for considerable levels of morbidity and mortality.[2] Therefore, APAP-induced acute toxicity has become an essential model for studying drug-induced liver and kidney failure. In the liver, APAP overdose produces centrilobular hepatic necrosis that can be fatal as it progresses to fulminant liver failure.[6] However, despite substantial progress in understanding APAP-induced hepatotoxicity,[7–9] additional injurious mechanisms responsible for the cellular damage induced by APAP remain unknown.

At normal dosage, the major elimination pathways of APAP involve glucuronide and sulfate conjugation. The initial step in toxicity is bioactivation of APAP by cytochrome *P*450 2e1 (Cyp2e1) to an electrophilic metabolite, *N*-acetyl-*p*-aminobenzoquinone imine (NAPQI).[10] At therapeutic doses, NAPQI is detoxified by glutathione (GSH) and eliminated in urine or bile as APAP-cysteine, APAP-*N*-acetylcysteine and APAP-APAP-GSH.[11] After an overdose, glucuronidation and sulfation routes become saturated and more extensive bioactivation of APAP occurs, leading to rapid depletion of

[1]Instituto de Investigaciones Biomédicas Alberto Sols (CSIC-UAM), Madrid 28029, Spain; [2]Centro de Investigación Biomédica en Red de Diabetes y Enfermedades Metabólicas Asociadas (CIBERDEM), ISCIII, Madrid, Spain; [3]Instituto de Ciencia y Tecnología de Alimentos y Nutrición (ICTAN-CSIC), Madrid 28040, Spain; [4]Centro de Investigación Biomédica en Red de Enfermedades Neurodegenerativas (CIBERNED), ISCIII, Madrid, Spain; [5]Section of Clinical Pharmacology and Toxicology, Arkansas Children's Hospital, Little Rock, AR 72207, USA; [6]Division of Clinical and Surgical Sciences, University of Edinburgh, Edinburgh EH164TJ, UK; [7]Oncology Surgery, Cell Therapy and Transplant Organs, Institute of Biomedicine of Seville (IBiS)/Virgen del Rocio Universitary Hospital/CSIC/University of Seville, Sevilla, Spain and [8]Centro de Investigación Biomédica en Red de Enfermedades Hepáticas y Digestivas (CIBERhed), Instituto de Salud Carlos III, Madrid, Spain
*Corresponding author: AM Valverde, Instituto de Investigaciones Biomédicas Alberto Sols (CSIC-UAM), Consejo Superior de Investigaciones Científicas c/Arturo Duperier 4, Madrid 28029, Spain. Tel: +34 915854497; Fax: +34 915854401; E-mail: avalverde@iib.uam.es
**Keywords:** liver injury; apoptosis; oxidative stress; survival signaling; tyrosine phosphorylation
**Abbreviations:** PTP1B, protein tyrosine phosphatase 1B; APAP, acetaminophen; JNK, c-jun (NH2) terminal kinase; Nrf2, nuclear factor-erythroid 2-related factor; IGFIR, insulin-like growth factor I receptor; ALT, alanine amino transaminase; GPx, glutathione peroxidase; GR, glutathione reductase; HO-1, heme oxigenase; GCL-C, γ-glutamyl cysteine ligase catalytic subunit; GCL-M, γ-glutamyl cysteine ligase modulatory subunit; SKF, Src kinase family
Received 05.1.13; revised 15.3.13; accepted 28.3.13; Edited by M Piacentini

the hepatic GSH pool. Subsequently, NAPQI binds to cysteine groups on cellular proteins forming APAP–protein adducts. NAPQI also binds to mitochondrial proteins, which, in turn, causes oxidative stress that may trigger signaling pathways through mitochondrial toxicity, leading to lethal cell injury. Moreover, generation of reactive oxygen (ROS) and nitrogen species, lipid peroxidation, mitochondrial dysfunction, disruption of calcium homeostasis and induction of apoptosis and necrosis are also involved in APAP-induced hepatotoxicity.[12–14] Therefore, tight control of ROS levels by antioxidant molecules and detoxifying enzymes is important to restore the balance between oxidants and antioxidants in cells challenged with oxidative insults. In this regard, nuclear factor erythroid-2-related factor 2 (Nrf2) activates detoxifying enzymes by binding to antioxidant response elements (AREs). Nrf2-deficient mice are highly susceptible to APAP-induced liver injury.[15] Thus, Nrf2 may serve as an endogenous regulator by which cells combat oxidative stress.

Protein tyrosine phosphorylation is crucial in the mechanisms by which growth factors and hormones regulate cellular metabolism, differentiation, growth and survival. Given the importance in maintaining survival and death fates of cells, the balance between tyrosine kinases and phosphatases is carefully regulated. Protein tyrosine phosphatases (PTPs) catalyze dephosphorylation of tyrosine-phosphorylated proteins.[16] Among them, protein tyrosine phosphatase 1B (PTP1B) is a widely expressed non-receptor PTP, which is associated with the endoplasmic reticulum by interaction through the C-terminal domain.[17] PTP1B has been proposed as a therapeutic target against type 2 diabetes and obesity via its capacity to dephosphorylate insulin and leptin receptors.[18,19] PTP1B also dephosphorylates and inactivates receptors of the tyrosine kinase superfamily, such as EGF receptor, PDGF receptor,[20] hepatocyte growth factor receptor/met [21] and insulin-like growth factor-I receptor (IGFIR),[22] which are involved in hepatocyte survival.[23,24] On this basis, the aim of this study was to investigate the role of PTP1B in APAP-induced hepatotoxicity.

## Results

**PTP1B expression increased during APAP-induced liver injury in human liver and APAP-treated human hepatocytes.** We investigated if PTP1B was modulated during APAP-induced human liver injury. Figure 1a shows elevated PTP1B in surviving hepatocytes, mainly in the areas surrounding the central veins (middle panel), during APAP intoxication as compared with a normal liver (left panel). In a more severe intoxication (right panel), where it is difficult to detect surviving hepatocytes, strong staining was observed in precipitated proteins released from dead cells and not yet cleared. PTP1B protein content was also upregulated in human primary hepatocytes and in the human Chang liver cell line (CHL) treated with APAP in a dose- and time-dependent manner (Figures 1b and c and Supplementary Figure 1). Elevation of PTP1B was detected at 8 h after APAP addition, whereas cells with death morphology were visualized at 16 h. Moreover, in APAP-treated human hepatocytes activation of c-jun (NH2) terminal kinase (JNK) and p38 mitogen-activated protein kinase (p38 MAPK) and inhibition of Akt phosphorylation correlated with decreased levels of the antiapoptotic Bcl2 family members BclxL and Mcl1 and with detection of the active caspase-3 fragment (Figure 1d).

**PTP1B-deficient mouse hepatocytes are protected against APAP-induced necrotic and apoptotic cell death.** As observed in human hepatocytes (Figure 1c), PTP1B was upregulated in primary hepatocytes from wild-type ($PTP1B^{+/+}$) mice treated with APAP (10 mM) at 8 h, whereas maximal cell death was observed at 16 h (Figure 2a). Next, we explored APAP-induced hepatotoxicity in mouse primary hepatocytes from wild-type and $PTP1B^{-/-}$ mice. Cells were treated with 5 and 10 mM APAP for 16 h and cell death was analyzed. Phase-contrast microscopy revealed many APAP-treated wild-type primary hepatocytes with cell death morphology. Conversely, most of $PTP1B^{-/-}$ primary hepatocytes remained attached to the plate and only few cells displayed a death phenotype (Figure 2b). Quantification analysis of crystal violet staining and released lactate dehydrogenase (LDH) activity showed that primary $PTP1B^{-/-}$ hepatocytes were more protected against APAP-induced necrotic cell death. Moreover, APAP treatment also increased the incidence of condensed and/or fragmented nuclei and the percentage of hypodiploid (sub-$G_0/G_1$) population in wild-type primary hepatocytes indicating apoptotic cell death (Figure 2c). These effects were reduced in $PTP1B^{-/-}$ cells. Apoptosis in APAP-treated wild-type primary hepatocytes correlated with the release of cytochrome *C* from the mitochondrial compartment and with the subsequent activation of caspase-3 (Figure 2d). These effects were significantly ameliorated in $PTP1B^{-/-}$ primary hepatocytes. Similar results were obtained using wild-type and $PTP1B^{-/-}$ immortalized hepatocytes that express comparable levels of pro- and antiapoptotic proteins than primary hepatocytes and are highly sensitive to APAP-induced cell death[25] (Supplementary Figure 2).

**Effect of PTP1B deficiency on the activation of stress- and survival-mediated signaling pathways in mouse hepatocytes.** Next, we analyzed stress- and survival-mediated signaling in primary hepatocytes from wild-type and $PTP1B^{-/-}$ mice in response to APAP. JNK and p38 MAPK phosphorylation was detected at 8 h in primary hepatocytes treated with 10 mM APAP, this effect being ameliorated in $PTP1B^{-/-}$ cells (Figure 3a). Survival signaling monitored by IGFIR phosphorylation, levels of insulin receptor substrates 1 (IRS1) and 2 (IRS2) and Akt phosphorylation, was reduced in APAP-treated wild-type primary hepatocytes, but preserved in $PTP1B^{-/-}$ cells. Consistently, the antiapoptotic markers BclxL and Mcl1 were decreased in wild-type primary hepatocytes treated with APAP but, again, this effect was reduced in $PTP1B^{-/-}$ hepatocytes. Similar responses were found in immortalized hepatocytes that activate stress kinases at lower APAP doses (Figure 3b).

To exclude the possibility that the protection elicited by PTP1B deficiency against APAP-induced cell death could be secondary to compensatory adaptations in $PTP1B^{-/-}$ hepatocytes, we established siRNA assays. Reduction of

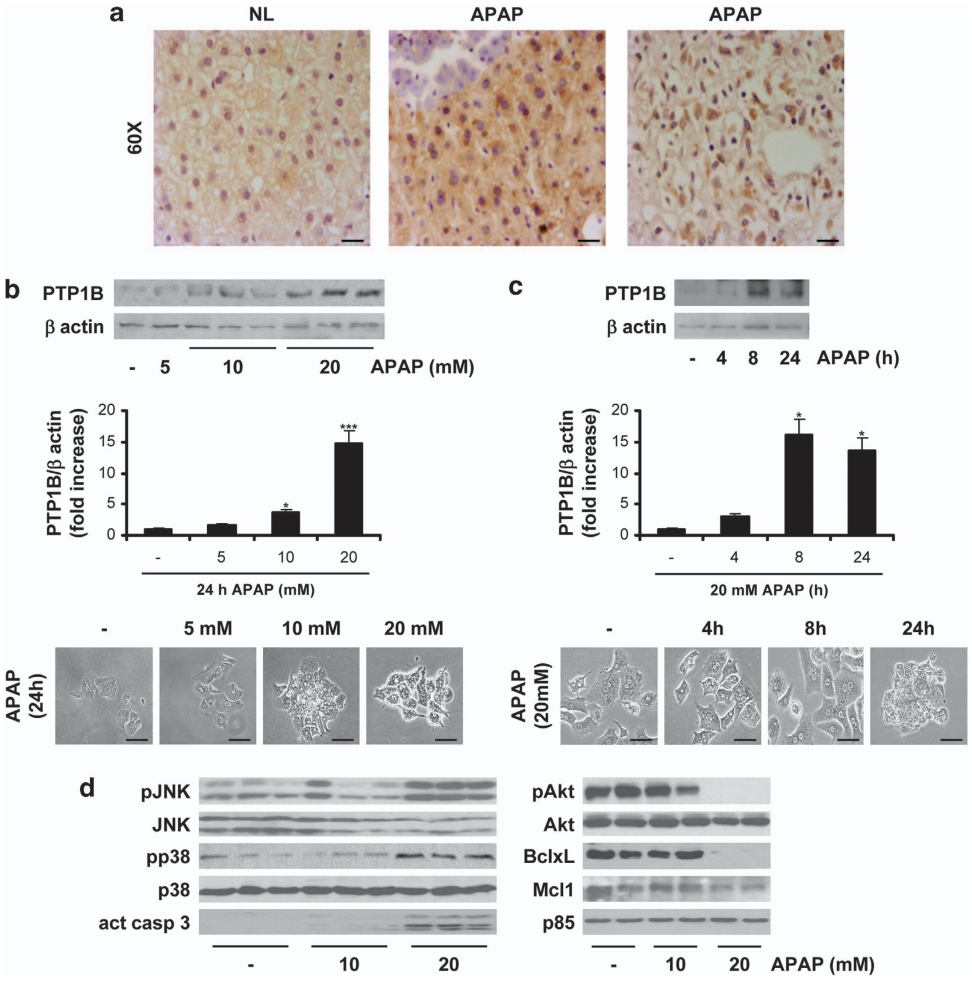


**Figure 1** PTP1B expression is increased during APAP-induced liver injury and in human primary hepatocytes treated with APAP. (**a**) Representative anti-PTP1B immunostaining of liver biopsy sections from patients with histologically normal liver (NL) or with an APAP overdose (APAP) ($n=7$). Bar = 50 $\mu$m. (**b**) Human primary hepatocytes were treated with various doses of APAP (5–20 mM) for 24 h. Total cell lysates were analyzed by western blot with the antibodies against PTP1B and $\beta$-actin as a loading control. Autoradiograms corresponding were quantitated by scanning densitometry. Results are means ± S.E.M. *$P<0.05$ and ***$P<0.005$ APAP-treated *versus* non-treated cells. Representative phase-contrast microscopy images after APAP treatment. Bar = 100 $\mu$m. (**c**) Human primary hepatocytes were treated with 20 mM APAP for various time-periods (4, 8 and 24 h). Total cell lysates were analyzed by western blot with the antibodies against PTP1B and $\beta$-actin as a loading control. Autoradiograms corresponding were quantitated by scanning densitometry. Results are means ± S.E.M. *$P<0.05$ APAP-treated *versus* non-treated cells. Representative phase-contrast microscopy images after APAP treatment. Bar = 100 $\mu$m. (**d**) Human primary hepatocytes were treated with various doses of APAP for 24 h and total cell lysates were analyzed by western blot with the antibodies against phospho (p)-JNK1/2, JNK1/2, phospho-p38, p38, active caspase-3, phospho-Akt, Akt, BclxL, Mcl1 and p85-PI3K as a loading control. *$P<0.05$ and ***$P<0.005$ APAP-treated *versus* non-treated cells ($n=3$ independent experiments)

PTP1B in wild-type immortalized hepatocytes decreased APAP-induced JNK phosphorylation and levels of the active caspase-3 fragment, and also maintained IGFIR tyrosine phosphorylation, IRS1 and IRS2 expression, Akt phosphorylation and abolished downregulation of BclxL upon APAP treatment (Figure 3c).

**PTP1B deficiency protects mouse hepatocytes against GSH depletion and elevation of ROS by prolonging Nrf2 nuclear accumulation.** In the liver, Cyp2e1 converts APAP to NAPQI that depletes GSH and, therefore, the degree of GSH consumption is a biomarker for APAP bioactivation.[26] As the expression of Cyp2e1 did not change in primary and immortalized hepatocytes from both genotypes of mice (Supplementary Figure 3), we used immortalized cells for further experiments. APAP induced depletion of GSH in wild-type immortalized hepatocytes after 4 h, and this effect was absent in PTP1B$^{-/-}$ cells (Figure 4a). Likewise, a significant elevation of ROS was detected in APAP-treated wild-type hepatocytes for 6 h, but not in PTP1B$^{-/-}$ cells. Next, we measured the enzymatic activity of the detoxifying enzymes glutathione peroxidase (GPx) and glutathione reductase (GR). GPx activity increased in APAP-treated wild-type hepatocytes compared with untreated controls, as expected for an antioxidant defense system. Conversely, GR was not increased by APAP, suggesting impairment in pathways replenishing GSH stores. PTP1B$^{-/-}$ hepatocytes did not activate the GPx/GR system in response to APAP, probably due to an insufficient threshold to trigger the activation of detoxifying enzymes under these experimental conditions.

To investigate at the molecular level the mechanisms for protection of PTP1B deficiency against APAP-induced

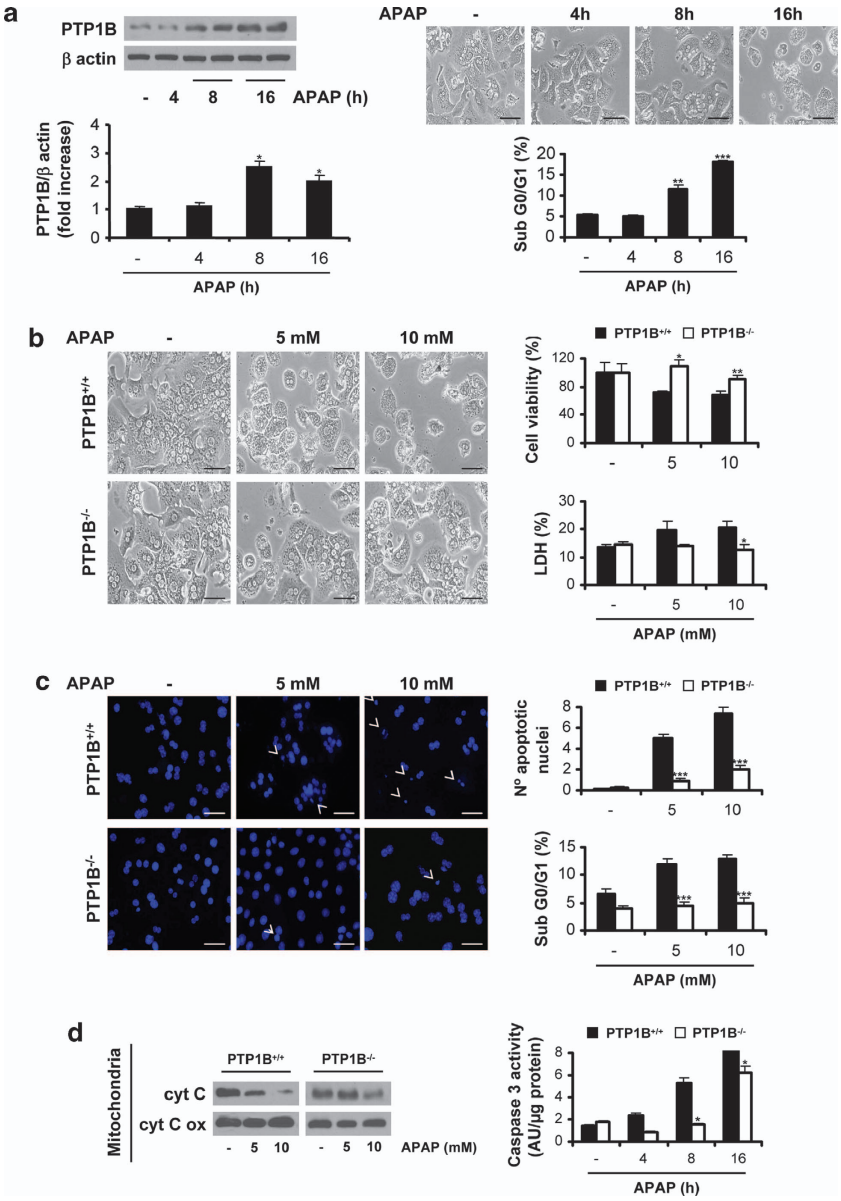


**Figure 2** PTP1B-deficient primary hepatocytes are protected against APAP-induced cell death. (**a**, left panel) Wild-type ($PTP1B^{+/+}$) mouse primary hepatocytes were treated with 10 mM APAP for various time-periods. The expression of PTP1B was analyzed by western blot. $^{*}P<0.05$ APAP-treated *versus* non-treated cells ($n=3$ independent experiments). (Right panel) Representative phase-contrast microscopy images and analysis of the percentage of sub-G0/G1 cell population by flow cytometry. (**b**) $PTP1B^{+/+}$ and $PTP1B^{-/-}$ primary hepatocytes were treated with APAP (5 and 10 mM) for 16 h. (Left panel) Representative phase-contrast microscopy images. Bar = 100 $\mu$m. (Right panel) Cellular viability and released LDH activity. (**c**) $PTP1B^{+/+}$ and $PTP1B^{-/-}$ primary hepatocytes were treated with APAP (5 and 10 mM) for 16 h. (Left panel) Representative nuclear morphology images after DAPI staining and analysis by fluorescence microscopy. (Right panel) Quantification of apoptotic nuclei. Percentage of sub-$G_0/G_1$ cell population analyzed by flow cytometry. (**d**, left panel) $PTP1B^{+/+}$ and $PTP1B^{-/-}$ primary hepatocytes were treated with APAP (5 and 10 mM) for 16 h. Western blot with anticytochrome *C* and anti-cytochrome *C* oxidase antibodies in mitochondrial extracts. (Right panel) $PTP1B^{+/+}$ and $PTP1B^{-/-}$ primary hepatocytes were treated with APAP (10 mM) for various time-periods. Analysis of caspase-3 enzymatic activity. $^{*}P<0.05$, $^{**}P<0.01$ and $^{***}P<0.005$ $PTP1B^{-/-}$ *versus* $PTP1B^{+/+}$ ($n=4$ independent experiments)

oxidative stress, we analyzed the dynamics of Nrf2 nuclear accumulation. As no differences in Nrf2 serine phosphorylation that dissociates Nrf2 to its inhibitor Keap1 at early time-periods upon APAP treatment were found (Supplementary Figure 4A), we analyzed the nuclear accumulation of Nrf2 at later time-periods. Western blot and immunofluorescence revealed that Nrf2 was maximally accumulated in the nucleus at 8 h after APAP treatment in wild-type and $PTP1B^{-/-}$ hepatocytes, but was retained for up to 16 h exclusively in $PTP1B^{-/-}$ cells (Figure 4b). Nuclear Nrf2 accumulation was accompanied by decreases in cytosolic expression (Supplementary Figure 4B).

Tyrosine phosphorylation of Nrf2 results in its nuclear export, ubiquitination and degradation in the cytosol.[27] Figure 4c shows that in APAP-treated wild-type hepatocytes, maximal Nrf2 tyrosine phosphorylation was observed at 8 h and total Nrf2 protein content decreased at 16 h. In $PTP1B^{-/-}$ cells, maximal Nrf2 tyrosine phosphorylation

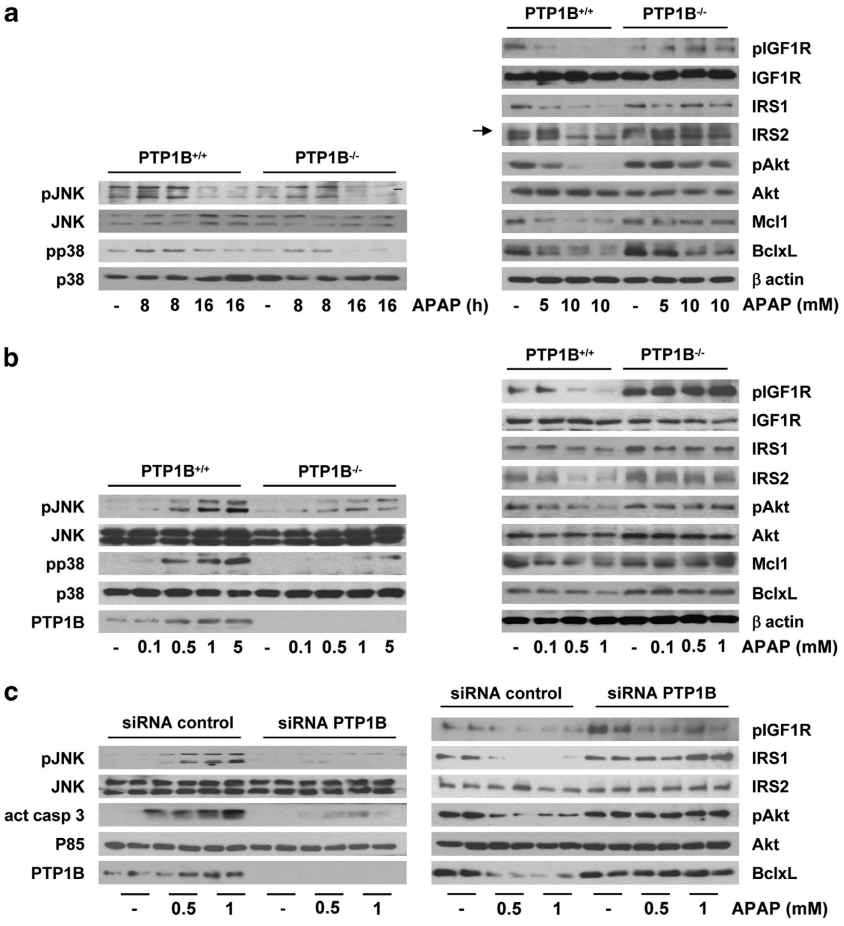


**Figure 3** Effect of PTP1B deficiency in stress and survival signaling in hepatocytes. (**a**, left panel) PTP1B$^{+/+}$ and PTP1B$^{-/-}$ mouse primary hepatocytes were treated with APAP (10 mM) for various time periods. Total cell lysates were analyzed by western blot with the antibodies against phospho (p)-JNK1/2, JNK1/2, phospho-p38 MAPK and p38 MAPK. Representative autoradiograms corresponding to three independent experiments are shown. (Right panel) PTP1B$^{+/+}$ and PTP1B$^{-/-}$ mouse primary hepatocytes were treated with APAP (5 and 10 mM) for 16 h. Total cell lysates were analyzed by western blot with the antibodies against phospho (p)-IGFIR, IGFIR, IRS1, IRS2, phospho-Akt, Akt, BclxL, Mcl1 and $\beta$-actin as a loading control. Representative autoradiograms corresponding to three independent experiments are shown. (**b**) PTP1B$^{+/+}$ and PTP1B$^{-/-}$ immortalized hepatocytes were treated with various doses of APAP for 16 h. Total cell lysates were analyzed by western blot with the indicated antibodies. Representative autoradiograms corresponding to three independent experiments are shown. (**c**) Immortalized PTP1B$^{+/+}$ hepatocytes transfected with 10 nM of control or PTP1B small interfering RNA (siRNA) for 48 h were further treated with various doses of APAP for 16 h. Total cell lysates were analyzed by western blot with the indicated antibodies. Representative autoradiograms corresponding to three independent experiments are shown

occurred at 16 h, a time-point at which total Nrf2 levels were maintained as in non-treated cells. These data correlated with greater increase in the expression of the Nrf2 target heme oxygenase-1 (HO-1) in PTP1B$^{-/-}$ hepatocytes. As occurred in immortalized hepatocytes, Nrf2 levels were maintained and the induction of HO-1 was higher in APAP-treated mouse primary PTP1B$^{-/-}$ hepatocytes for 16 h as compared with the wild-type cells.

Next, ubiquitination analysis of Nrf2 was performed in immortalized hepatocytes treated with APAP for 8–24 h either in the absence or presence of the proteasome inhibitor MG132 (Figure 4d). In APAP-treated wild-type cells, ubiquitinated Nrf2 was detected at earlier time-points (8 h) compared with PTP1B$^{-/-}$ cells, which displayed this response at 16 h; this effect was enhanced when APAP was added with MG132. In related experiments, overexpression of PTP1B in HEK 293T cells inhibited ARE-mediated luciferase expression after treatment with APAP for 16 h (Figure 4e), reinforcing the involvement of PTP1B in Nrf2-mediated antioxidant response to APAP.

**PTP1B modulates GSK3$\beta$/SKF-mediated Nrf2 nuclear accumulation in APAP-treated mouse hepatocytes.** In response to oxidative stress, GSK3$\beta$ is activated by phosphorylation at Tyr216 by an unknown tyrosine kinase. Activated GSK3$\beta$ phosphorylates and activates Src kinase family (SKF) members in the cytosol, allowing their nuclear translocation and subsequent tyrosine phosphorylation of Nrf2 at Tyr568, ultimately resulting in Nrf2 nuclear exclusion and degradation.[27,28] We examined if this molecular mechanism was triggered in APAP-treated hepatocytes. Silencing GSK3$\beta$ in immortalized wild-type hepatocytes (Supplementary Figure 5) prolonged Nrf2 nuclear accumulation up to 24 h upon APAP treatment as observed in PTP1B$^{-/-}$ cells (Figures 4b and 5a). Moreover, nuclear translocation of Fyn and Src was also impaired in GSK3$\beta$-silenced cells, although no effects of nuclear translocation of Yes were observed (results not shown). To reinforce the role of SKF in nuclear accumulation of Nrf2 in response to APAP, we treated wild-type hepatocytes with the

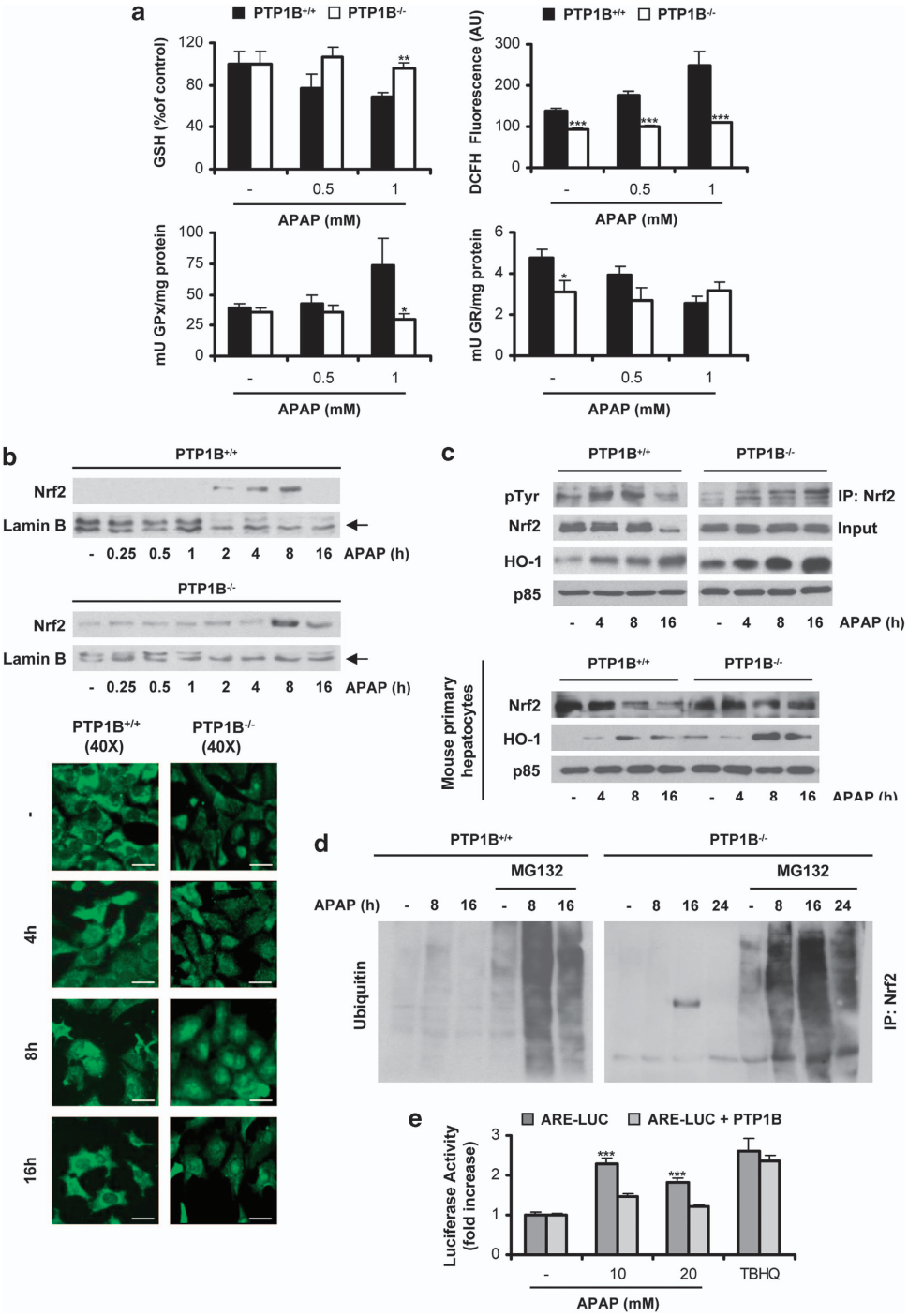


**Figure 4** PTP1B deficiency protects hepatocytes against GSH depletion and elevation of ROS; effect on nuclear Nrf2 accumulation. PTP1B$^{+/+}$ and PTP1B$^{-/-}$ immortalized hepatocytes were treated with various doses of APAP for different time-periods. (**a**) Analysis of GSH content (4 h), ROS levels (6 h) and GPx and GR activity (16 h) in three independent experiments. *$P<0.05$, **$P<0.01$ and ***$P<0.005$ PTP1B$^{-/-}$ *versus* PTP1B$^{+/+}$ (**b**, upper panel) Analysis of Nrf2 in nuclear cell lysates by western blot in PTP1B$^{+/+}$ and PTP1B$^{-/-}$ immortalized hepatocytes treated with 1 mM APAP for several time-periods. Representative autoradiograms of three to four independent experiments are shown. (Lower panel) Representative images corresponding to the intracellular localization of Nrf2 by immunofluorescence microscopy in PTP1B$^{+/+}$ and PTP1B$^{-/-}$ immortalized hepatocytes treated with 1 mM APAP for several time-periods. Bar = 50 $\mu$m. (**c**) (Upper panel) PTP1B$^{+/+}$ and PTP1B$^{-/-}$ immortalized hepatocytes were treated with 1 mM APAP for several time-periods. Nrf2 tyrosine phosphorylation was analyzed by immunoprecipitation with the anti-Nrf2 antibody, followed by western blot with the anti-Tyr(P) antibody. Total Nrf2 and HO-1 was analyzed by western blot. (Lower panel) PTP1B$^{+/+}$ and PTP1B$^{-/-}$ mouse primary hepatocytes were treated with 10 mM APAP for various time-periods. Total Nrf2 and HO-1 was analyzed by western blot. (**d**) PTP1B$^{+/+}$ and PTP1B$^{-/-}$ immortalized hepatocytes were treated with MG132 (10 nM) for 30 min, and then with 1 mM APAP for different time-periods. Whole-cell lysates were analyzed by immunoprecipitation with anti-Nrf2 antibody, followed by western blot with anti-ubiquitin antibody. (**e**) Antioxidant response element (ARE)-mediated luciferase activity was measured in HEK 293T cells transfected with the expression vectors for pcDNA3.1mNrf2-V5/HisB and 3 × ARE-Luc combined with myc-PTP1B only in the indicated cases and treated with various doses of APAP for 16 h. tBHQ (15 $\mu$M) was used as a positive control ($n=3$ independent experiments performed in triplicate). ***$P<0.005$ PTP1B-transfected (Nrf2 ARE + PTP1B) *versus* empty vector-transfected (Nrf2 ARE) cells

SKF inhibitor PP2. As shown in Figure 5b, PP2 increased nuclear Nrf2 levels at 2–8 h after APAP treatment. In addition, in mouse embryonic fibroblasts (MEFs) deficient in SKF ($SYF^{-/-}$) treated with APAP Nrf2 was accumulated in the nucleus up to 24 h.

We next analyzed the effect of PTP1B deficiency on the GSK3$\beta$/SKF signaling pathway. In wild-type cells, APAP-induced GSK3$\beta$ tyrosine phosphorylation was detected at 1 h and peaked at 4 h. This response paralleled the re-entry of Fyn and Src into the nucleus (Figure 5c). In $PTP1B^{-/-}$ hepatocytes, maximal GSK3$\beta$ phosphorylation occurred later at 8–16 h after APAP treatment and also paralleled the re-entry of Src and Fyn into the nucleus as observed in wild-type cells.

**PTP1B-deficient mice are protected against APAP-induced oxidative stress through the enhancement of Nrf2 nuclear accumulation.** Increased survival was observed in $PTP1B^{-/-}$ mice injected with an APAP overdose (300 mg/kg) as compared with the wild-type control (Figure 6a). Consistently, serum alanine transaminase (ALT) was sevenfold higher in wild-type mice than in $PTP1B^{-/-}$ mice at 6 and 24 h after injection (Figure 6b). Of note, necrotic lesions were observed exclusively in livers of wild-type mice (Figure 6c). Next, we analyzed the hepatic expression of proinflammatory cytokines. At 6 h after APAP injection, elevated IL6 and IL1$\beta$ mRNA levels were found in livers of wild-type mice, but not in $PTP1B^{-/-}$ animals (Figure 6d). APAP decreased TNF$\alpha$ mRNA levels in

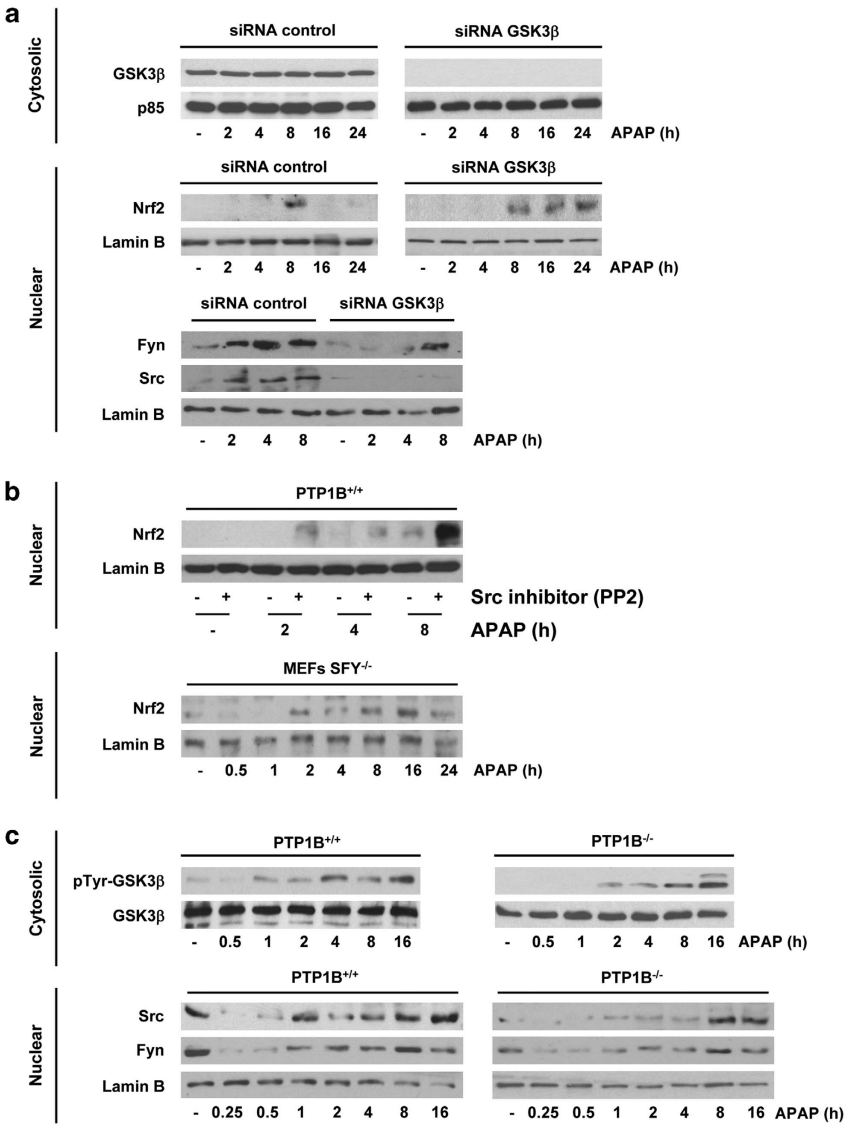


**Figure 5** PTP1B modulates GSK3$\beta$/Src-Fyn-mediated Nrf2 nuclear accumulation in APAP-treated hepatocytes. (**a**) $PTP1B^{+/+}$ immortalized hepatocytes were transfected with control or GSK3$\beta$ small interfering RNAs (siRNAs) (25 nM) for 48 h, followed by stimulation with 1 mM APAP. Nuclear and cytosolic extracts were analyzed by western blot with antibodies against Nrf2, Fyn and Src. (**b**, upper panel) $PTP1B^{+/+}$ immortalized hepatocytes were treated with PP2 (5 $\mu$M) for 30 min following 1 mM APAP for different periods. Nrf2 in nuclear extracts was analyzed by western blot. (Lower panel) $SYF^{-/-}$ MEFs were treated with 1 mM APAP for different periods and Nrf2 was analyzed in nuclear extracts by western blot. (**c**) $PTP1B^{+/+}$ and $PTP1B^{-/-}$ immortalized hepatocytes were treated with 1 mM APAP for different periods. Phosphorylated GSK3β (Tyr216) was analyzed in cytosolic extracts by western blot. Fyn and Src were analyzed in nuclear extracts. Similar results were obtained in three independent experiments

wild-type, but not in PTP1B-deficient mice. As hepatic PTP1B expression is modulated by inflammation,[29] we performed the immunohistochemistry analysis. Increased PTP1B staining was found in necrotic lesions of APAP-treated wild-type mice after 6 h, particularly in areas surrounding the central veins, but no signs of liver injury were observed in sections from PTP1B$^{-/-}$ mice (Figure 6e). We next determined if reduced sensitivity of PTP1B$^{-/-}$ mice to APAP-induced liver injury was associated with alterations in GSH levels. APAP administration depleted GSH at 3 and 6 h and increased APAP–protein adducts, these effects being significantly ameliorated in the PTP1B$^{-/-}$ group (Figure 6f). Protein carbonyl levels, an indicator of tissue oxidative stress, were less elevated in APAP-injected PTP1B$^{-/-}$ mice than in wild-type mice and paralleled the reduced GSH depletion.

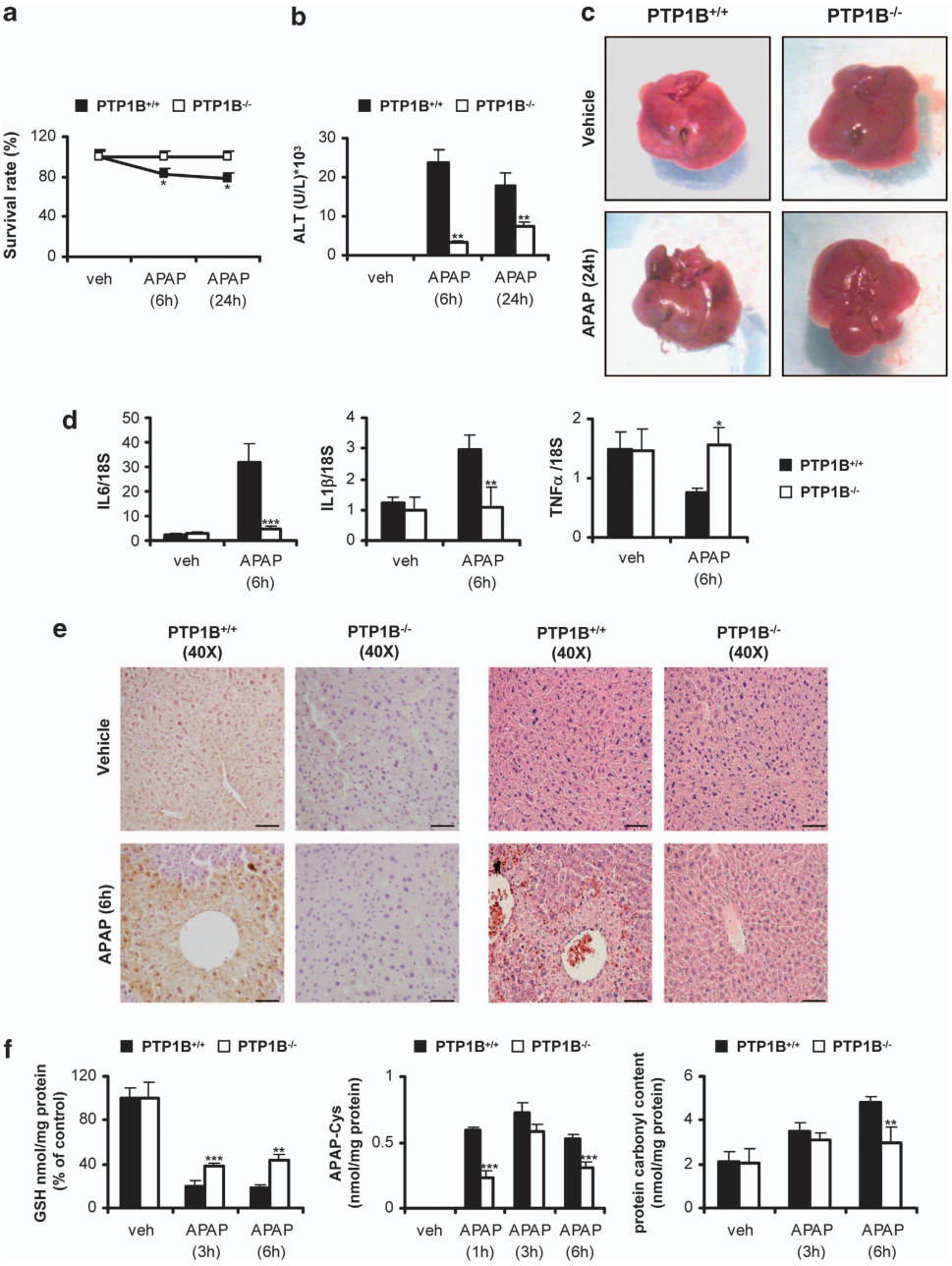


**Figure 6** PTP1B-deficient mice are protected against APAP-induced, inflammation oxidative stress and liver damage. PTP1B$^{+/+}$ and PTP1B$^{-/-}$ mice were injected with 300 mg/kg APAP or saline for 6 or 24 h. (**a**) Survival curves after 24 h of APAP injection. (**b**) ALT activity at 6 and 24 h. (**c**) Representative images of whole livers from PTP1B$^{+/+}$ and PTP1B$^{-/-}$ mice 24 h after APAP injection. (**d**) IL6, IL1$\beta$ and TNF$\alpha$ mRNA levels were determined by real-time polymerase chain reaction in livers from PTP1B$^{+/+}$ and PTP1B$^{-/-}$ mice at 6 h after APAP injection. (**e**) Representative anti-PTP1B immunostaining (left panel) and hematoxylin and eosin staining (right panel) in livers from PTP1B$^{+/+}$ and PTP1B$^{-/-}$ mice 6 h after APAP injection. Bar = 100 $\mu$m. (**f**) GSH (left panel), APAP–protein adducts (middle panel) and carbonylated protein levels (right panel) were analyzed in livers from PTP1B$^{+/+}$ and PTP1B$^{-/-}$ mice at various time-periods after APAP injection. *$P<0.05$, **$P<0.01$ and ***$P<0.005$ PTP1B$^{-/-}$ *versus* PTP1B$^{+/+}$ ($n=6$–8 mice of each condition). Cys, cysteine. Veh, vehicle

As intracellular redox state is chiefly regulated by Nrf2, we examined differences in nuclear levels of Nrf2 *in vivo.* Nuclear Nrf2 was detected in livers of wild-type mice at 3 and 6 h after APAP treatment (Figure 7a). In PTP1B$^{-/-}$ animals, basal nuclear Nrf2 was detected before APAP administration and increased at 3 and 6 h after injection, where the levels were higher than those of control mice. Similarly, APAP-induced HO-1 protein content was higher in PTP1B$^{-/-}$ mice. Then, we analyzed additional Nrf2 target genes. mRNA levels of GPx, HO-1 and $\gamma$-glutamyl cysteine ligase modulatory subunit (GCL-M) significantly increased at 3-h after APAP injection in livers of PTP1B$^{-/-}$ mice as compared with the wild-type and GPx, $\gamma$-glutamyl cysteine ligase catalytic subunit (GCL-C), GCL-M and NAD(P)H quinone oxidoreductase 1 (NQO1) mRNA increased at 6 h (Figure 7b).

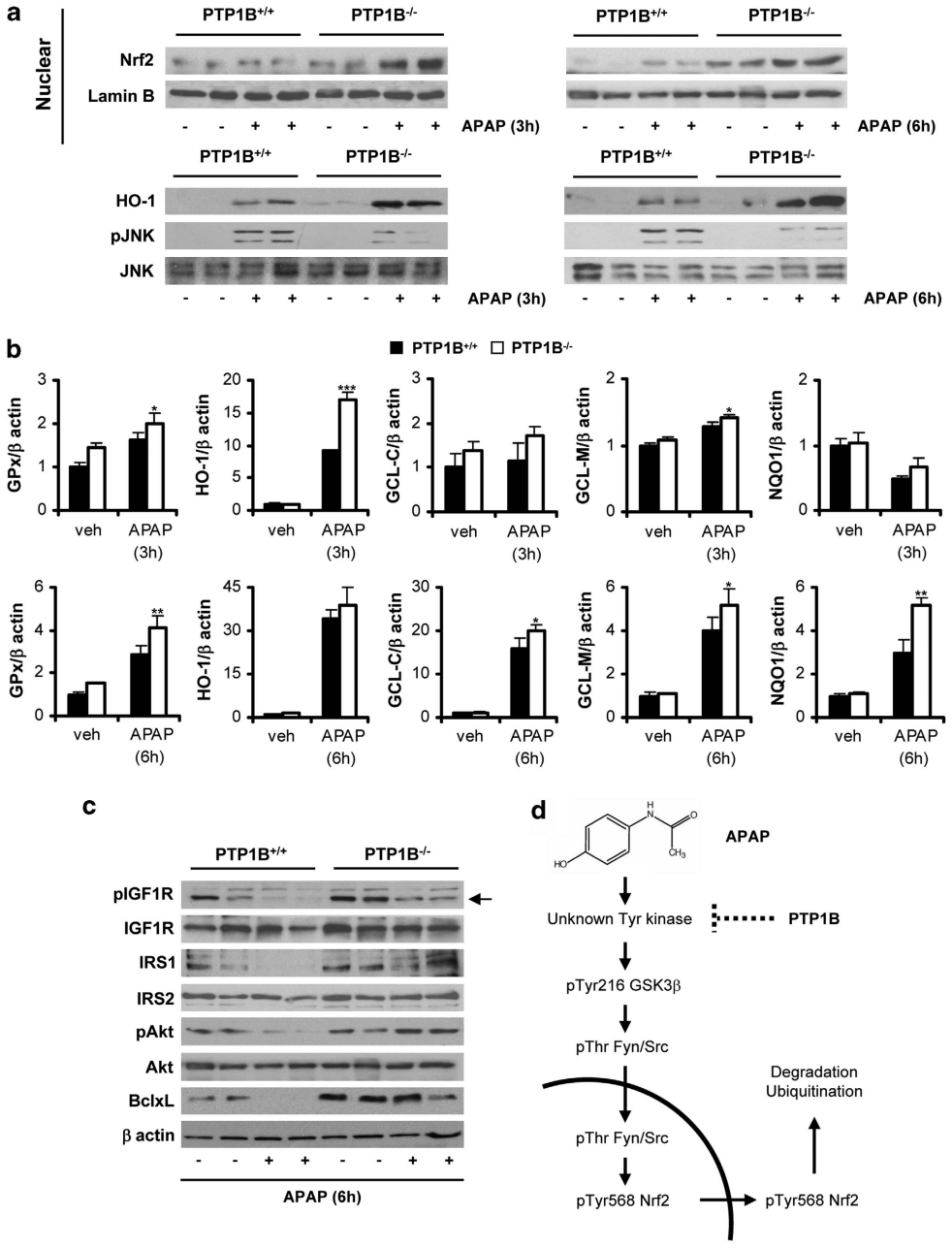


**Figure 7** Beneficial effects of PTP1B deficiency on the induction of Nrf2-mediated antioxidant response and survival signaling in the liver. PTP1B$^{+/+}$ and PTP1B$^{-/-}$ mice were injected with 300 mg/kg APAP or saline for 3 or 6 h. (**a**) Western blot analysis of Nrf2 in nuclear extracts and HO-1, phospho (p)-JNK and JNK in total liver extracts. (**b**) GPx, HO-1, GCL-M, GCL-C and NQO1 mRNA levels determined by quantitative real-time polymerase chain reaction (qRT-PCR) at 3 and 6 h after APAP injection. *$P<0.05$, **$P<0.01$ and ***$P<0.005$ PTP1B$^{-/-}$ *versus* PTP1B$^{+/+}$ ($n=6$–8 mice of each condition). (**c**) Western blot analysis of phospho (p)-IGFIR, IGFIR, IRS1, IRS2, phospho-Akt, Akt and BclxL levels in total liver extracts from PTP1B$^{+/+}$ and PTP1B$^{-/-}$ mice 6 h after APAP injection. (**d**) Schematic diagram illustrating the proposed mechanism by which PTP1B modulates Nrf2 nuclear accumulation. PTP1B might activate the unknown kinase upstream GSK3$\beta$ by dephosphorylation, thereby triggering activation of the GSK3$\beta$/Src-Fyn axis in the nucleus that ultimately leads to Nrf2 tyrosine phosphorylation, ubiquitination and degradation. Veh, vehicle

**Decreased JNK activation and sustained IGFIR/Akt/BclxL survival signaling in APAP-treated PTP1B-deficient mice.** Activation of JNK was detected in APAP-treated wild-type mice at 3 and 6 h after injection. As expected, this effect decreased in PTP1B$^{-/-}$ mice (Figure 7a). Regarding survival signaling, in wild-type mice IGFIR phosphorylation was severely reduced at 6 h after APAP injection and IRS1 protein levels were downregulated in parallel with decreased Akt phosphorylation (Figure 7c). Consistently, antiapoptotic BclxL protein was barely detected at 6 h after APAP injection. Conversely, APAP-treated PTP1B$^{-/-}$ mice maintained IGFIR and Akt phosphorylation, as well as IRS1 and BclxL protein content to similar levels than those of mice injected with saline.

## Discussion

There is evidence of increased PTP1B expression during the progression of non-alcoholic fatty liver disease that concurs with insulin resistance and liver damage.[30,31] However, PTP1B functions in physiological responses regulated by tyrosine kinase signaling, such as hepatocellular survival during drug injury, are poorly understood. Our results have unraveled a central role of PTP1B in the molecular mechanism that mediates APAP-induced liver failure, identifying PTP1B as a potential therapeutic target in the treatment of human APAP hepatotoxicity. This study emerged from the observation of elevated PTP1B expression in livers from individuals suffering from APAP intoxication. Importantly, in APAP-treated human and mouse hepatocytes, upregulation of PTP1B preceded cell death.

Results in mouse hepatocytes demonstrated that PTP1B deficiency attenuates cellular damage in response to APAP. The fact that released LDH activity was reduced in PTP1B$^{-/-}$ hepatocytes indicates that necrotic cell death was less severe than in wild-type cells. In wild-type hepatocytes, APAP also increased the percentage of sub-G0/G1 cells and release of cytochrome *C* from the mitochondria. APAP also induced activation of caspase-3 and decreased expression of antiapoptotic proteins BclxL and Mcl1. These results strongly suggest that APAP also triggered apoptosis in hepatocytes and, again, these effects were ameliorated by PTP1B deficiency. The role of apoptosis in APAP-induced hepatocyte cell death is controversial. However, there are studies that clearly demonstrate both types of cell death following APAP overdose. Circulating apoptotic and necrotic cell death markers have been detected in patients with APAP-induced acute liver injury.[32–34] Cell death via necrosis and apoptosis has been reported in the livers removed during transplantation because of APAP intoxication.[35] These data have also been shown in mice during APAP poisoning.[36] In light of these results, we and others have shown that PTP1B inhibition protects hepatocytes against activation of mitochondrial (intrinsic) and death receptor (extrinsic)-mediated apoptotic pathways,[21,25] reinforcing the role of this phosphatase in programmed cell death.

As cellular oxidative stress processes (GSH depletion and ROS generation)[13] are ameliorated in PTP1B$^{-/-}$ hepatocytes, we investigated the modulation of oxidative stress by PTP1B. An unknown tyrosine kinase has been proposed to be the upstream activator of GSK3$\beta$ by phosphorylation at Tyr216.[27,28] This phenomenon leads to SKF-mediated tyrosine phosphorylation, nuclear export, ubiquitination and degradation of Nrf2 in response to oxidative stress inducers. Our data demonstrated firstly that this signaling pathway is activated by APAP in hepatocytes and secondly that PTP1B deficiency mimics the inhibition of GSK3$\beta$ or SKF on the downstream mediators of this pathway. Inhibition of GSK3$\beta$ or SKF augmented and prolonged Nrf2 nuclear accumulation, delaying its nuclear exclusion in response to APAP. Importantly, the effect of PTP1B deficiency on this pathway was manifested by delayed Src-Fyn nuclear translocation, Nrf2 tyrosine phosphorylation and its subsequent ubiquitination and degradation, leading to enhanced HO-1 induction. These results suggest that PTP1B might activate this unknown kinase upstream from GSK3$\beta$, probably by dephosphorylation, and thereby triggering the activation of the GSK3$\beta$/Src-Fyn axis that ultimately leads to Nrf2 degradation. Consequently, as demonstrated in hepatocytes, PTP1B deficiency might delay and/or reduce activation of this complex axis, resulting in prolonged nuclear accumulation of Nrf2 and enhanced antioxidant defense.

Besides the novel role of PTP1B in antioxidant defense reported herein, this phosphatase regulates duration and/or intensity of survival signals emerging from the tyrosine kinase receptor family.[19–21] As IGFIR triggers survival responses in hepatocytes,[37] the lack of PTP1B prevented the reduction in IGFIR/IRS1/2/Akt-mediated survival signaling in APAP-treated cells. In fact, this is the first report showing degradation of IRS proteins in hepatocytes by APAP, suggesting that high doses of this analgesic may also interfere with hepatic insulin signaling and increase the risk of metabolic diseases such as type 2 diabetes mellitus. Thus, in wild-type hepatocytes, increased ROS-mediated JNK and p38 MAPK phosphorylation by APAP are likely to be responsible for the feedback mechanism on IGFIR-mediated signaling, leading to IRS1/2 serine phosphorylation that precedes degradation.[38] In the absence of PTP1B, the decrease in ROS-mediated activation of JNK and p38 MAPK and the increase in IGFIR tyrosine phosphorylation might act in conjunction with the effects on the GSK3$\beta$/Src-Fyn axis, resulting in attenuated oxidative stress and increased cell survival in response to APAP.

Several studies have shown the mechanistic importance of hepatic cytokines in APAP-induced liver injury. In the liver, cytokines are mainly produced by non-parenchymal cells. Our *in vivo* data show significant lower expression levels of IL1$\beta$ and IL6 mRNAs in the livers of PTP1B$^{-/-}$ mice upon APAP injection as compared with the elevated levels of the wild-type controls, suggesting that PTP1B also modulates cytokine production by non-parenchymal (i.e. Kupffer) cells in response to liver damage. Cytokines have an essential role as inducers of PTP1B in metabolic diseases. Activation of JNK together with elevated expression of PTP1B in response to IL6 has been reported in skeletal muscle of insulin-resistant mice.[39] Likewise, IL4 induces PTP1B to suppress IL4-induced STAT6 signaling in B cells.[40] As PTP1B is increased in the livers of APAP-injected wild-type mice, this effect is likely to be due to elevation of IL6 and IL1$\beta$. Therefore, cytokine-mediated increases in PTP1B expression might enhance the GSK3$\beta$/Src-Fyn axis, resulting in increased Nrf2 tyrosine phosphorylation and a rapid nuclear exclusion. Moreover, in the liver of APAP-injected wild-type mice, the negative

cross-talk elicited by JNK on IRS proteins and also by PTP1B by direct dephosphorylation of the IGFIR might synergize with the enhancement of the GSK3$\beta$/Src-Fyn axis to reduce survival of hepatocytes *in vivo*. This mechanism is supported by lower activation of JNK, higher IGFIR tyrosine phosphorylation and nuclear Nrf2 accumulation in livers of APAP-injected PTP1B$^{-/-}$ mice as compared with the wild-type controls. As a result, PTP1B-deficient livers are protected against APAP-induced oxidative stress and injury as manifested by decreased GSH depletion favoring NAPQI detoxification and subsequently limiting the formation of APAP–protein adducts. However, the effects of APAP *in vivo* are not exclusively mediated by elevation of PTP1B expression induced by proinflammatory cytokines secreted by non-parenchymal cells; our *in vitro* data have also demonstrated direct effects of APAP in hepatocytes. Nevertheless, PTP1B deficiency protects against damage in hepatocytes in culture and in whole liver, reinforcing the regulatory role of this phosphatase in multiple molecular mechanisms triggered in response to APAP in distinct liver cells.

As summarized in Figure 7d, we have demonstrated the unique role of PTP1B in the liver as a critical crossroad in the signaling pathways triggered in response to APAP by dual modulation of the Nrf2-mediated antioxidant response through the GSK3$\beta$/Src-Fyn kinases axis and the survival signaling through its effects on the IGFIR/IRSs/Akt signaling pathway. Collectively, our data suggest that inhibition of PTP1B would be a suitable therapeutic approach against APAP-induced hepatotoxicity.

## Materials and Methods

**Reagents and antibodies.** Fetal bovine serum and culture media were obtained from Invitrogen (Carlsbad, CA, USA). Protein A agarose was purchased from Roche Diagnostics. APAP and MG132 were from Sigma-Aldrich (St. Louis, MO, USA). PP2 was purchased from Tocris Bioscience (Ellsville, MO, USA). The antibodies used in this study were: anti-cleaved (Asp175) caspase-3 (no. 9661), anti-phospho-JNK (Thr183/Tyr185) (no. 4668), anti-phospho-p38 MAPK (Thr180/Tyr182) (no. 9211), anti-p38 MAPK (no. 9212), anti-Akt (no. 9272), and anti-ubiquitin (no. 3936) antibodies were from Cell Signaling Technology (Danvers, MA, USA). Anti-Bclx (no. 610211), anti-phospho-GSK3$\beta$ (no. 612312), anti-GSK3$\beta$ (no. 6102019) and anti-cytochrome *C* (no. 556433) antibodies were from BD Biosciences (San Diego, CA, USA). Anti-phospho-IGF-IR (Tyr1165/1166) (sc-101704), anti-JNK (sc-571), anti-phospho-Akt1/2/3 (Ser473) (sc-7985-R), anti-Nrf2 (C-20, sc-722), anti-Mcl1 (sc-819), anti-Fyn (sc-16), anti-Keap1 (sc-33569), anti-Lamin B (sc-20682 in Figure 4b) and anti-human PTP1B (sc-14021) were from Santa Cruz Biotechnology (Palo Alto, CA, USA). The anti-IRS1 (06-248), anti-IRS2 (06-506), anti-p85$\alpha$ (06-195), anti-mouse PTP1B (07-088), anti-HO1 (AB1284), anti-phospho-Ser (clone 4A4, 05-1000X) and anti-phospho-Tyr (clone 4G10, 05-321) antibodies were purchased from Merck Millipore (Merck KGaA, Darmstadt, Germany). Anti-IGF-IR antibody was a gift from S Pons (CSIC, Madrid, Spain). Anti-$\beta$-actin (A-5441) antibody was from Sigma Chemical Co. (St. Louis, MO, USA). Anti-Lamin B (aB16048) and anti-Cyp2e1 antibody (aB19140) were from Abcam (Cambridge, UK). Mouse monoclonal antibody (mAb) 327 against c-Src was from Calbiochem (Merck KGaA, Darmstadt, Germany). Anti-cytochrome *C* oxidase subunit I antibody (A-6403) was from Molecular Probes (Eugene, OR, USA).

**Human liver biopsies.** Human liver samples were obtained from the Department of Pathology, University of Edinburgh (Edinburgh, UK). Written informed consent was obtained from each patient. Characteristics of five patients transplanted following APAP overdose are shown in Table 1.

**Animal models.** Three-month-old male PTP1B$^{+/+}$ (wild-type) and PTP1B$^{-/-}$ mice on the C57Bl/6J $\times$ 129Sv/J genetic background and maintained as described previously[41] were used throughout this study. Animal experimentation was approved by the ethic committee at CSIC and was conducted according to the accepted guidelines for animal care of the Comunidad de Madrid (Spain). Overnight fasted mice were intraperitoneally (i.p.) injected with 300 mg/kg APAP dissolved in physiological saline. Mice were killed at 1, 3, 6 and 24 h and livers and blood were collected.

**Cell culture.** Human hepatocytes were prepared from liver biopsies obtained from 12 patients (eight male, four female aged 58 $\pm$ 4.0 years) submitted to a surgical resection for liver tumors after obtaining patients' written consent. Hepatocytes' isolation was based on the two-step collagenase procedure.[42] Mouse hepatocytes were isolated from male mice (8–12 weeks old) by perfusion with collagenase and cultured as described.[41] CHLs, purchased from the ATCC, (Manassas, VA, USA) were a gift from P Martin-Sanz (CSIC). The generation and characterization of immortalized hepatocyte cell lines from wild-type and PTP1B$^{-/-}$ mice has been described previously.[43] Cells were grown in DMEM plus 10% heat-inactivated fetal calf serum and stimulated with various doses of APAP.

**Liver histology.** Histological grading of hepatic necrosis was performed by two blinded observers using hematoxylin and eosin (H&E)-stained sections as follows: 30% of the total area necrotic (one point); 30–60% of the total area necrotic (two points); and 60% of the total area necrotic (three points). PTP1B immunohistochemistry was performed as described previously.[44]

**Analysis of ALT activity.** Blood was collected in tubes containing heparin and diluted 1/30 with saline (0.9% NaCl). ALT activity was determined by direct measurement with the Reflotron test (Ref. 10745120; Roche Diagnostics, Indianapolis, IN, USA).

**Transient transfection with siRNA.** siRNA oligonucleotides were synthesized by Dharmacon RNAi Technologies (Fisher Scientific-USA, Pittsburgh, PA, USA) for gene silencing of mouse PTP1B and GSK3$\beta$. Wild-type immortalized hepatocytes were seeded in 6-cm dishes and incubated overnight at 37 °C with 5% $CO_2$. When 40–50% confluence was reached, cells were transfected with 10 nM of PTP1B or 25 nM GSK3$\beta$ siRNAs or with a scrambled control siRNA following DharmaFECT General Transfection Protocol. After 48 h, cells were used for experiments.

**Immunofluorescence.** Cells were grown in glass coverslips until 80% confluence was reached. Then, cells were washed two times with PBS, fixed in methanol ($-20$ °C) for 2 min and processed to immunofluorescence. Primary anti-Nrf2 antibody was applied for 1 h at 37 °C in PBS–1% bovine serum albumin (BSA), followed by 4 $\times$ 5 min washes in PBS, a 45-min incubation with fluorescence-conjugated secondary antibody (Alexa 488 goat anti-rabbit) and

**Table 1** Demographic and biochemical characteristics of patients with APAP hepatotoxicity

| Patient number | Age (years) | Sex | Acetaminophen dose | Staggered overdose | Admission alanine aminotransferase (IU/l) | Admission creatinine ($\mu$mol/l) | Prothrombin time (s) | Overdose to transplant (h) |
|---|---|---|---|---|---|---|---|---|
| 1 | 42 | Female | 32 g | No | 12755 | 218 | 77 | 212 |
| 2 | 43 | Female | NA | NA | 7106 | 192 | 182 | NA |
| 3 | 48 | Male | 16 g | Yes | 20800 | 124 | 96 | NA |
| 4 | 45 | Female | 10 g | No | 1097 | 142 | 69 | 176 |
| 5 | 36 | Male | 50 g | No | 9847 | 152 | 87 | 70 |

NA, not available
Normal range alanine aminotransferase 10–50 IU/l, creatinine 60—120 $\mu$mol/l and prothrombin time 10.2–12.7 s

four final washes of 5 min each in PBS. Immunofluorescence was examined in a Nikon Eclipse 90i microscope (Nikon Instruments, Inc., Melville, NY, USA). Immunofluorescence mounting medium was from Vector Laboratories Inc. (Burlingame, CA, USA). For 4,6-diamidino-2-phenylindole (DAPI) staining, cells were washed with PBS, fixed in methanol ( − 20 °C) for 2 min and stained with 1 $\mu$M DAPI for 5 min in the dark. After washing with PBS, nuclear morphology was analyzed by fluorescence microscopy.

**Evaluation of cell viability by LDH leakage assay.** Cellular damage was evaluated by LDH leakage assay as described.[45]

**Analysis of cellular viability by crystal violet.** After cell incubation with APAP, the medium was discarded, and the remaining viable adherent cells were stained with crystal violet (0.2% (w/v) in 2% ethanol) for 20 min. After this time, plates were rinsed with tap water and allowed to dry, and 1% SDS was added to solubilize them. The absorbance of each plate was read spectrophotometrically at 560 nm. Dishes without cells were processed in parallel to correct the nonspecific adhesion of crystal violet to the plastic. The remaining viable cells were calculated as the percentage of absorbance with respect to control cells (incubated in the absence of APAP).

**Quantification of apoptotic cells by flow cytometry.** After induction of apoptosis, adherent and non-adherent cells were collected by centrifugation, washed with PBS and fixed with cold ethanol. The cells were then washed, resuspended in PBS and incubated with RNAse A (25 $\mu$g/10$^6$ cells) for 30 min at 37 °C. After addition of 0.05% propidium iodide, cells were analyzed by flow cytometry.

**Analysis of caspase-3 activity.** Cells were scraped off, collected by centrifugation at 2500 × *g* for 5 min and lysed at 4 °C in 5 mM Tris/HCl (pH 8), 20 mM EDTA and 0.5% Triton X-100. Caspase-3 activity was determined as described previously.[25] Protein concentration of cell lysates was determined, and the results are presented as caspase-3 activity per micrograms of total protein.

**Luciferase assays.** HEK 293T cells were seeded on 24-well plates (100 000 cells per well), cultured for 16 h and transfected using calcium phosphate. Transient transfections of HEK 293T cells were performed with the expression vectors for pcDNA3.1mNrf2-V5/HisB (a gift from Dr. JD Hayes, Biomedical Research Institute, Ninewells Hospital and Medical School, University of Dundee, Dundee, UK), *Renilla* (Promega, Madison, WI, USA) and 3 × ARE-Luc (a gift from Dr. J Alam, Department of Molecular Genetics, Ochsner Clinic Foundation, Baton Rouge, LA, USA) combined with myc-PTP1B (a gift from Dr. M Tremblay, Department of Biochemistry, McGill University, Montreal, QC, Canada) only in the indicated cases. After transfection, cells were treated with vehicle (PBS), APAP (10 and 20 mM) or *tert*-butyl hydroquinone (*t*BHQ) (15 $\mu$M) for 16 h. Cells were lysed and assayed for luciferase activity with the dual luciferase assay system (Promega), according to the manufacturer's instructions. Relative light units were measured in a GloMax 96 microplate luminometer with dual injectors (Promega, Madison, WI, USA).

**Homogenization and preparation of tissue extracts.** Frozen livers were homogenized in 16 volumes (w/v) of ice-cold lysis buffer containing 50 mM Tris-HCl, 1% Triton X-100, 2 mM EGTA, 10 mM EDTA acid, 100 mM NaF, 1 mM $Na_4P_2O_7$, 2 mM $Na_3VO_4$, 100 $\mu$g/ml phenylmethylsulfonyl fluoride (PMSF), 1 $\mu$g/ml aprotinin, 1 $\mu$g/ml pepstatin A and 1 $\mu$g/ml leupeptin. Livers were homogenized in the same lysis buffer using the Brinkman PT 10/35 Polytron (American Laboratory Trading, Inc. East Lyme, CT, USA). Extracts were kept ice-cold at all times. Liver extracts were cleared by microcentrifugation at 40 000 × *g* for 20 min at 4 °C. The supernatant was aliquoted and stored at − 70 °C.

**Protein determination.** Protein determination was performed by the Bradford dye method, using the Bio-Rad reagent and BSA as the standard.

**Immunoprecipitations and western blot.** To obtain total cell lysates, cells from supernatants were collected by centrifugation at 2000 × *g* for 5 min at 4 °C. Attached cells were scraped off in ice-cold PBS, pelleted by centrifugation at 4000 × *g* for 10 min at 4 °C and resuspended in lysis buffer (25 mM HEPES, 2.5 nM EDTA, 0.1% Triton X-100, 1 mM PMSF and 5 $\mu$g/ml leupeptin). Cellular lysates were clarified by centrifugation at 12 000 × *g* for 10 min. After protein content determination, equal amounts of protein (600 $\mu$g–1 mg) were immunoprecipitated at 4 °C with the corresponding antibodies. The immune complexes were collected on agarose beads and submitted to western blot analysis. After SDS-PAGE, gels were transferred to Immobilon membranes and were blocked using 5% non-fat dried milk or 3% BSA in 10 mM Tris-HCl, 150 mM NaCl (pH 7.5) and incubated overnight with antibodies as indicated in 0.05% Tween-20, 10 mM Tris-HCl and 150 mM NaCl (pH 7.5). Immunoreactive bands were visualized using the ECL Western blotting protocol (Millipore).

**Extraction of nuclear and cytosolic proteins.** Cells and liver were resuspended at 4 °C in 10 mM HEPES-KOH (pH 7.9), 1.5 mM $MgCl_2$, 10 mM KCl, 0.5 mM DTT, 0.2 mM PMSF, 0.75 $\mu$g/ml leupeptin, 0.75 $\mu$g/ml aprotinin (Buffer A), allowed to swell on ice for 10 min, and then vortexed for 10 s. Samples were centrifuged and the supernatant containing the cytosolic fraction was stored at − 70 °C. The pellet was resuspended in cold buffer C (20 mM HEPES-KOH (pH 7.9), 25% glycerol, 420 mM NaCl, 1.5 mM $MgCl_2$, 0.2 mM EDTA, 0.5 mM DTT, 0.2 mM PMSF, 0.75 $\mu$g/ml leupeptin, 0.75 $\mu$g/ml aprotinin) and incubated on ice for 20 min for high salt extraction. Cellular debris was removed by centrifugation for 2 min at 4 °C, and the supernatant fraction was stored at − 70 °C.

**Isolation of mitochondrial and cytosolic extracts.** At the end of the culture time, cells were recovered by scrapping and collected by centrifugation at 2500 × *g* for 5 min at 4 °C. Mitochondrial and cytosolic extracts were obtained as described previously.[25]

**Determination of GSH.** The content of GSH was quantified by the fluorometric assay of Hissin and Hilf.[46]

**Determination of GPx and GR enzymatic activities.** Cells were collected in PBS and centrifuged at low speed (300 × *g*) for 5 min to pellet cells. Cell pellets were resuspended in 20 mM Tris containing 5 mM EDTA and 0.5 mM mercaptoethanol, submitted to ultrasound and centrifuged at 3000 × *g* for 15 min. Enzyme activities were measured in the supernatants as described.[47]

**Measurement of intracellular ROS.** For visualization and analysis of intracellular ROS by flow cytometry, the oxidation-sensitive DCFH-DA probe was used. Cells were detached by trypsinization and the cellular fluorescence intensity was measured after 30-min incubation with 5 $\mu$M DCFH-DA by using a FACScan flow cytometer (BD Biosciences, San José, CA, USA). For each analysis, 10 000 events were recorded.

**Determination of protein carbonyl content.** Protein oxidation of liver homogenates was measured as carbonyl groups' content according to the method of Richert *et al.*[48]

**Determination of APA–protein adducts.** Analysis of APAP covalently bound to proteins in liver was measured by initial protease treatment of liver homogenates, followed by high-performance liquid chromatography-electrochemical analysis for APAP-cysteine as described previously.[49]

**Quantitative real-time PCR analysis and primer sequence.** Total RNA was extracted with Trizol (Invitrogen) and reverse transcribed using a SuperScriptTM III First-Strand Synthesis System for qPCR following the manufacturer's indications (Invitrogen). qPCR was performed with an ABI 7900 sequence detector (Invitrogen) using the SyBr Green method and d(N)$_6$ random hexamer with the primers indicated in Supplementary Table 1. Primer-probe sets for mouse PTP1B, TNF$\alpha$, IL6 and IL1$\beta$ were purchased as predesigned TaqMan gene expression assays (Applied Biosystems, Life Technologies, Carlsbad, CA, USA).

**Data analysis.** Data are expressed as mean ± S.E.M. Comparisons between groups were made using one-way ANOVA. For qRT-PCR, a two-way ANOVA test followed by a Bonferroni's post-test was used. Differences were considered to be statistically significant at $P<0.05$. The data were analyzed with the SPSS (windows statistical package, version 9.0.1, SPSS Inc., Chicago, IL, USA).

## Conflict of Interest

The authors declare no conflict of interest.

**Acknowledgements**. We acknowledge the following grant support: SAF2012-33283 (MINECO, Spain), Comunidad de Madrid S2010/BMD-2423, EFSD and Amylin Paul Langerhans Grant and Centro de Investigación Biomédica

en Red de Diabetes y Enfermedades Metabólicas Asociadas (CIBERDEM, ISCIII, Spain) (to AMV); SAF2012-38048 (MINECO, Spain) (to JM-P); PI09/0185 and Centro de Investigación Biomédica en Red de Enfermedades Hepáticas y Digestivas (CIBEREHD, ISCIII, Spain) (to JM); AGL2010-17579 (MINECO, Spain) (to LG); and SAF2010-17822 (MINECO, Spain) (to AC).

1. Rumack BH. Acetaminophen misconceptions. *Hepatology* 2004; **40**: 10–15.
2. Lee WM. Acetaminophen and the U.S. Acute Liver Failure Study Group: lowering the risks of hepatic failure. *Hepatology* 2004; **40**: 6–9.
3. Litovitz TL, Klein-Schwartz W, White S, Cobaugh DJ, Youniss J, Omslaer JC *et al.* 2000 Annual report of the American Association of Poison Control Centers Toxic Exposure Surveillance System. *Am J Emerg Med 2001* **19**: 337–395.
4. Lee WM. Acetaminophen toxicity: changing perceptions on a social/medical issue. *Hepatology* 2007; **46**: 966–970.
5. Kaplowitz N. Acetaminophen hepatoxicity: what do we know, what don't we know, and what do we do next? *Hepatology* 2004; **40**: 23–26.
6. Ramachandran R, Kakar S. Histological patterns in drug-induced liver disease. *J Clin Pathol* 2009; **62**: 481–492.
7. James LP, Mayeux PR, Hinson JA. Acetaminophen-induced hepatotoxicity. *Drug Metab Dispos* 2003; **31**: 1499–1506.
8. Jaeschke H, Bajt ML. Intracellular signaling mechanisms of acetaminophen-induced liver cell death. *Toxicol Sci* 2006; **89**: 31–41.
9. Han D, Shinohara M, Ybanez MD, Saberi B, Kaplowitz N. Signal transduction pathways involved in drug-induced liver injury. *Handb Exp Pharmacol* 2010; **196**: 267–310.
10. Thummel KE, Lee CA, Kunze KL, Nelson SD, Slattery JT. Oxidation of acetaminophen to *N*-acetyl-*p*-aminobenzoquinone imine by human CYP3A4. *Biochem Pharmacol* 1993; **45**: 1563–1569.
11. Newton JF, Hoefle D, Gemborys MW, Mudge GH, Hook JB. Metabolism and excretion of a glutathione conjugate of acetaminophen in the isolated perfused rat kidney. *J Pharmacol Exp Ther* 1986; **237**: 519–524.
12. Ghosh A, Sil PC. Protection of acetaminophen induced mitochondrial dysfunctions and hepatic necrosis via Akt-NF-kappaB pathway: role of a novel plant protein. *Chem Biol Interact* 2009; **177**: 96–106.
13. Reid AB, Kurten RC, McCullough SS, Brock RW, Hinson JA. Mechanisms of acetaminophen-induced hepatotoxicity: role of oxidative stress and mitochondrial permeability transition in freshly isolated mouse hepatocytes. *J Pharmacol Exp Ther* 2005; **312**: 509–516.
14. Jaeschke H, McGill MR, Ramachandran A. Oxidant stress, mitochondria, and cell death mechanisms in drug-induced liver injury: lessons learned from acetaminophen hepatotoxicity. *Drug Metab Rev* 2012; **44**: 88–106.
15. Enomoto A, Itoh K, Nagayoshi E, Haruta J, Kimura T, O'Connor T *et al.* High sensitivity of Nrf2 knockout mice to acetaminophen hepatotoxicity associated with decreased expression of ARE-regulated drug metabolizing enzymes and antioxidant genes. *Toxicol Sci* 2001; **59**: 169–177.
16. Tonks NK, Neel BG. Combinatorial control of the specificity of protein tyrosine phosphatases. *Curr Opin Cell Biol* 2001; **13**: 182–195.
17. Frangioni JV, Beahm PH, Shifrin V, Jost CA, Neel BG. The nontransmembrane tyrosine phosphatase PTP-1B localizes to the endoplasmic reticulum via its 35 amino acid C-terminal sequence. *Cell* 1992; **68**: 545–560.
18. Salmeen A, Andersen JN, Myers MP, Tonks NK, Barford D. Molecular basis for the dephosphorylation of the activation segment of the insulin receptor by protein tyrosine phosphatase 1B. *Mol Cell* 2000; **6**: 1401–1412.
19. Zabolotny JM, Bence-Hanulec KK, Stricker-Krongrad A, Haj F, Wang Y, Minokoshi Y *et al.* PTP1B regulates leptin signal transduction *in vivo*. *Dev Cell* 2002; **2**: 489–495.
20. Haj FG, Markova B, Klaman LD, Bohmer FD, Neel BG. Regulation of receptor tyrosine kinase signaling by protein tyrosine phosphatase-1B. *J Biol Chem* 2003; **278**: 739–744.
21. Sangwan V, Paliouras GN, Cheng A, Dube N, Tremblay ML, Park M. Protein-tyrosine phosphatase 1B deficiency protects against Fas-induced hepatic failure. *J Biol Chem* 2006; **281**: 221–228.
22. Buckley DA, Cheng A, Kiely PA, Tremblay ML, O'Connor R. Regulation of insulin-like growth factor type I (IGF-I) receptor kinase activity by protein tyrosine phosphatase 1B (PTP-1B) and enhanced IGF-I-mediated suppression of apoptosis and motility in PTP-1B-deficient fibroblasts. *Mol Cell Biol* 2002; **22**: 1998–2010.
23. Fabregat I, Herrera B, Fernandez M, Alvarez AM, Sanchez A, Roncero C *et al.* Epidermal growth factor impairs the cytochrome *C*/caspase-3 apoptotic pathway induced by transforming growth factor beta in rat fetal hepatocytes via a phosphoinositide 3-kinase-dependent pathway. *Hepatology* 2000; **32**: 528–535.
24. Valverde AM, Fabregat I, Burks DJ, White MF, Benito M. IRS-2 mediates the antiapoptotic effect of insulin in neonatal hepatocytes. *Hepatology* 2004; **40**: 1285–1294.
25. Gonzalez-Rodriguez A, Escribano O, Alba J, Rondinone CM, Benito M, Valverde AM. Levels of protein tyrosine phosphatase 1B determine susceptibility to apoptosis in serum-deprived hepatocytes. *J Cell Physiol* 2007; **212**: 76–88.
26. Kon K, Kim JS, Jaeschke H, Lemasters JJ. Mitochondrial permeability transition in acetaminophen-induced necrosis and apoptosis of cultured mouse hepatocytes. *Hepatology* 2004; **40**: 1170–1179.
27. Niture SK, Jain AK, Shelton PM, Jaiswal AK. Src subfamily kinases regulate nuclear export and degradation of transcription factor Nrf2 to switch off Nrf2-mediated antioxidant activation of cytoprotective gene expression. *J Biol Chem* 2011; **286**: 28821–28832.
28. Jain AK, Jaiswal AK. GSK-3beta acts upstream of Fyn kinase in regulation of nuclear export and degradation of NF-E2 related factor 2. *J Biol Chem* 2007; **282**: 16502–16510.
29. Zabolotny JM, Kim YB, Welsh LA, Kershaw EE, Neel BG, Kahn BB. Protein-tyrosine phosphatase 1B expression is induced by inflammation *in vivo*. *J Biol Chem* 2008; **283**: 14230–14241.
30. Sanderson SO, Smyrk TC. The use of protein tyrosine phosphatase 1B and insulin receptor immunostains to differentiate nonalcoholic from alcoholic steatohepatitis in liver biopsy specimens. *Am J Clin Pathol* 2005; **123**: 503–509.
31. Garcia-Monzon C, Lo Iacono O, Mayoral R, Gonzalez-Rodriguez A, Miquilena-Colina ME, Lozano-Rodriguez T *et al.* Hepatic insulin resistance is associated with increased apoptosis and fibrogenesis in nonalcoholic steatohepatitis and chronic hepatitis C. *J Hepatol* **54**: 142–152.
32. Bechmann LP, Jochum C, Kocabayoglu P, Sowa JP, Kassalik M, Gieseler RK *et al.* Cytokeratin 18-based modification of the MELD score improves prediction of spontaneous survival after acute liver injury. *J Hepatol* **53**: 639–647.
33. Antoine DJ, Jenkins RE, Dear JW, Williams DP, McGill MR, Sharpe MR *et al.* Molecular forms of HMGB1 and keratin-18 as mechanistic biomarkers for mode of cell death and prognosis during clinical acetaminophen hepatotoxicity. *J Hepatol May* **56**: 1070–1079.
34. Craig DG, Lee P, Pryde EA, Masterton GS, Hayes PC, Simpson KJ. Circulating apoptotic and necrotic cell death markers in patients with acute liver injury. *Liver Int* **31**: 1127–1136.
35. McGregor AH, More LJ, Simpson KJ, Harrison DJ. Liver death and regeneration in paracetamol toxicity. *Hum Exp Toxicol* 2003; **22**: 221–227.
36. Antoine DJ, Williams DP, Kipar A, Jenkins RE, Regan SL, Sathish JG *et al.* High-mobility group box-1 protein and keratin-18, circulating serum proteins informative of acetaminophen-induced necrosis and apoptosis *in vivo*. *Toxicol Sci* 2009; **112**: 521–531.
37. Tovar V, Alsinet C, Villanueva A, Hoshida Y, Chiang DY, Sole M *et al.* IGF activation in a molecular subclass of hepatocellular carcinoma and pre-clinical efficacy of IGF-1R blockage. *J Hepatol Apr* **52**: 550–559.
38. Vinayagamoorthi R, Bobby Z, Sridhar MG. Antioxidants preserve redox balance and inhibit c-Jun-N-terminal kinase pathway while improving insulin signaling in fat-fed rats: evidence for the role of oxidative stress on IRS-1 serine phosphorylation and insulin resistance. *J Endocrinol* 2008; **197**: 287–296.
39. Nieto-Vazquez I, Fernandez-Veledo S, de Alvaro C, Lorenzo M. Dual role of interleukin-6 in regulating insulin sensitivity in murine skeletal muscle. *Diabetes* 2008; **57**: 3211–3221.
40. Lu X, Malumbres R, Shields B, Jiang X, Sarosiek KA, Natkunam Y *et al.* PTP1B is a negative regulator of interleukin 4-induced STAT6 signaling. *Blood* 2008; **112**: 4098–4108.
41. Gonzalez-Rodriguez A, Mas Gutierrez JA, Sanz-Gonzalez S, Ros M, Burks DJ, Valverde AM. Inhibition of PTP1B restores IRS1-mediated hepatic insulin signaling in IRS2-deficient mice. *Diabetes* 2010; **59**: 588–599.
42. Pichard L, Raulet E, Fabre G, Ferrini JB, Ourlin JC, Maurel P. Human hepatocyte culture. *Methods Mol Biol* 2006; **320**: 283–293.
43. Gonzalez-Rodriguez A, Clampit JE, Escribano O, Benito M, Rondinone CM, Valverde AM. Developmental switch from prolonged insulin action to increased insulin sensitivity in protein tyrosine phosphatase 1B-deficient hepatocytes. *Endocrinology* 2007; **148**: 594–608.
44. Gonzalez-Rodriguez A, Mas-Gutierrez JA, Mirasierra M, Fernandez-Perez A, Lee YJ, Ko HJ *et al.* Essential role of protein tyrosine phosphatase 1B in obesity-induced inflammation and peripheral insulin resistance during aging. *Aging Cell* 2012; **11**: 284–296.
45. Welder AA Acosta D. (ed) *Enzyme Leakage As An Indicator of Cytotoxicity in Culture Cells*. Academic Press: New York, NY, USA, 1994, p 3.
46. Hissin PJ, Hilf R. A fluorometric method for determination of oxidized and reduced glutathione in tissues. *Anal Biochem* 1976; **74**: 214–226.
47. Rodriguez-Ramiro I, Martin MA, Ramos S, Bravo L, Goya L. Comparative effects of dietary flavanols on antioxidant defences and their response to oxidant-induced stress on Caco2 cells. *Eur J Nutr* **50**: 313–322.
48. Richert S, Wehr NB, Stadtman ER, Levine RL. Assessment of skin carbonyl content as a noninvasive measure of biological age. *Arch Biochem Biophys* 2002; **397**: 430–432.
49. Muldrew KL, James LP, Coop L, McCullough SS, Hendrickson HP, Hinson JA *et al.* Determination of acetaminophen–protein adducts in mouse liver and serum and human serum after hepatotoxic doses of acetaminophen using high-performance liquid chromatography with electrochemical detection. *Drug Metab Dispos* 2002; **30**: 446–451.



Supplementary Information accompanies this paper on Cell Death and Disease website (http://www.nature.com/cddis)